Microcellular Injection Molding of Foamed Engineering Plastic Parts with High Dimensional Accuracy

Yu-Teng Feng[a], *Haiying Zhan*[a], *Hao-Yang Mi*[a]*, *Maxwell Fordjour Antwi-Afari*[c], *Youfu Chen*[b], *Laifa Gu*[b], *Binbin Dong*[a]*, *Chuntai Liu*[a], *Changyu Shen*[a]

[a] National Engineering Research Center for Advanced Polymer Processing Technology, The Key Laboratory of Advanced Materials Processing & Mold of Ministry of Education, Zhengzhou University, Zhengzhou 450001, China

[b] Ningbo Shuanglin Auto Parts Co., Ltd, Ningbo, 315600, China

[c] Department of Civil Engineering, College of Engineering and Physical Sciences, Aston University, Birmingham, B4 7ET, United Kingdom

Corresponding Authors:

H.Y. Mi E-mail: mihaoyang@zzu.edu.cn

B. Dong E-mail: binbindong@zzu.edu.cn

Note:

The authors declare no competing financial interest.

Abstract

Polyformaldehyde (POM) and Polyamide 66 (PA66) are engineering plastics with excellent mechanical properties and thermal stability. Producing microcellular injection molded POM and PA66 parts with high dimensional accuracy would be beneficial to reduce material cost and product quality. In this research, foamed POM and PA66 gear parts were fabricated by using microcellular injection molding with supercritical nitrogen as the blowing agent. Compared to conventional injection molded parts (parts that foaming is not involved), the foamed POM and PA66 gear parts achieved 5% and 10% average weight reduction, respectively. The foamed parts displayed a lower shrinkage ratio when compared to the solid counterparts, which was attributed to the cell expansion that offset part of the inward shrinkage stress. Moreover, POM gear parts with a higher crystallinity degree presented more serious shrinkage ratio compared to the PA66 gear parts, which contributed to the denser polymer molecular chains arrangement. The shrinkage ratio in both directions of PA66 foamed gear parts depended on the injection volume, and the lowest shrinkage ratio of 0.043‰ was obtained at the injection volume of 74 mm, when the polymer reached the maximum foaming ratio. The findings from this study could provide practical guidance for preparing microcellular injection molded products with high dimensional accuracy.

Keywords: Microcellular injection molding; Shrinkage ratio; Cell morphology; Dimensional accuracy

1. Introduction

Thermoplastic engineering plastics are known for their chemical and abrasion resistance coupled with outstanding mechanical properties and thermal stability. Polymer gears like Polyoxymethylene (POM) and Polyamide 66 (PA66) have been widely used in industries such as automobile parts, electronic devices, household facilities, and medical instruments[1]. Compared to metallic gears, polymer gears possess highly specialized mechanical properties, tribological performance, load resistance and ability to reduce noise[2]. The main approaches to process these polymer gears include classical cutting processes and injection molding. Injection molding is considered one of the most effective means of mass production, which is less costly and highly automated[3,4]. However, the exceedingly high processing temperature makes it more difficult to produce engineering plastic products than other normal plastics[5,6]. In addition, the warpage and shrinkage of injection molded products are common challenging issues for manufacturers[7-9].

Introducing micron-sized cells into injection molded products is a practical method to achieve weight reduction and dimensional stability improvement. Microcellular plastics were first proposed at MIT in the 1980s by Professor Nam Suh[10]. Supercritical fluids (SCF) such as CO_2 or N_2 were always employed as the physical blowing agent (PBA) to produce microcellular structured parts with substantial micron-sized cells in the core layer. After blending SCF into polymer melt in a barrel, a single-phase gas/polymer solution was formed under the rotation of the screw[11]. The homogeneous solution was then injected into the cavity through the nozzle, which

triggered the nucleation and growth of micron-sized cells. This could be attributed to the pressure variation and sudden drop in temperature[12]. Compared to conventional injection molding techniques, microcellular injection molding possesses more advantages, including shorter cooling/cycle times, lower dimensional instability, and easy processing conditions. These merits made it a good choice to produce complicated and thick-wall injection molded parts[13].

Microcellular injection molding is a superior technology to produce various foamed plastics with complex shapes in many fields, and has numerous achievements in surface quality and dimension accuracy[14,15]. For instance, Guo et al. designed an in-mold decoration (IMD) method by attaching a PET film to the mold cavity whilst integrating the IMD with microcellular injection molding (MIM). Their results showed that compared to MIM, the PET film improves the surface quality by flattening the bubbles that have not been cooled and turned to the surface[16]. Chen et al. studied a variable mold temperature method to improve the surface quality of microcellular injection molded parts, finding that using induction heating to increase the mold surface temperature from 100 ℃ to 160 ℃ could decrease surface roughness of polycarbonate parts from 25 μm to 6.5 μm, and the flow marks were completely removed at a mold temperature of 160 ℃[17]. Shyh-Shin[18] et al. investigated the mechanical properties and dimensional stability of a microcellular injection molded gear shaft fabricated by PA66. Their results showed that dimensional stability was improved by microcellular injection molding. Hyun Keun Kim[19] et al. analyzed the fundamental principles and characteristics of the microcellular foaming process to minimize warpage in glass fiber

reinforced polymer. They found that the shrinkage difference in various directions would affect the warpage of microcellular plastics, and the warpage decreased significantly compared with the solid parts, especially in the direction perpendicular to the flow direction. Zafar et al. employed the ASTM standard rod-shaped parts fabricated by glass-fiber-filled and unfilled acetal copolymers, and found that the linear and volumetric shrinkage of both types gradually decreased with increasing weight reduction[20].

Hitherto, literature on improving the dimensional accuracy of injection molded products were mainly focused on the process conditions[21-23]. Research on minimizing shrinkage and warpage with microcellular injection molding is still insufficient, especially, researches on engineering plastics. For example, Kramschuster et al. studied the shrinkage and warpage characteristics of a box-shaped PP part using design of experiments (DOE), and confirmed that a reduction in the shrinkage and warpage could be achieved through the microcellular foaming process[24,25]. Guo et al. investigated the effects of processing parameters in microcellular injection molding to obtain lightweight plastic products with high dimensional accuracy for automotive industry, finding that initial gas concentration and melt temperature are the most significant parameters to warpage and shrinkage[26]. Introducing micron-sized cells in the production of POM and PA66 gear parts would be beneficial for reducing the part density, material cost, and cycle time. It is also a panacea for less shrinkage and lower dimensional instability. In the meantime, the detailed underlying mechanism affecting

the shrinkage of engineering plastic in microcellular injection molding deserves in-depth research.

In this research, a plastic gear with six gates was used to investigate the dimensional accuracy improvement of microcellular injection molding technique. The most widely used engineering plastics including POM and PA66 were selected as the raw materials to process the injection molded gears. The correlation and comparison of the microstructure, surface appearance, and shrinkage ratio were studied. The results showed that the surface roughness of foamed gear parts was a bit higher than the solid ones due to the silver streaks and swirl marks. Moreover, the foaming ratio in the region near the gate was more significant than in the region far from the gate. Additionally, the foamed gear displayed more precise dimensional accuracy in both flow direction and cross direction when compared with their solid counterparts, and the PA66 gears showed lower shrinkage ratio than the POM ones. The PA66 foamed gear presented a shrinkage reduction of 28% in the flow direction and a 42% reduction in the cross direction, which benefited from the expansion forces of micron-sized bubbles offsetting the shrinkage stress. Furthermore, the optimized process parameters were obtained by employing a suitable injection volume, which could achieve the minimum shrinkage ratio of 0.07‰.

2. Experimental Section

2.1 Materials

The POM pellets (M90-44) with glass transition of 162 ℃ and melting point of 166℃ were purchased from Polyplastics (Japan), and the PA66 pellets (101L) were provided by the Chimei, with the glass transition of 181 ℃ and melting point of 198 ℃. An injection molding machine (Arburg Allrounder 570S) equipped with a supercritical N_2 (scN_2) supply system (MuCell® Trexel) was applied to prepare porous POM and PA66 samples, the amount of N_2 injected was precisely controlled by adjusting the valve size and the valve open time of the N_2 supply system.

2.2 Microcellular Injection Molding of POM and PA66

The commercial-grade POM pallets were pre-dried at 80 ℃ for 2 hours in a vacuum oven to make sure the residual moisture was below 0.02 %. The optimal microcellular injection molding parameters were opted through multiple adjustments to process the injection molding gears, including the melting temperature, mold temperature, cooling time, and N_2 content, which were set as 210 ℃, 80 ℃, 50 s, and 0.50 %, respectively. For PA66 injection molding gears, the commercial-grade PA66 pallets were dried at 80 ℃ for 2 hours in a vacuum oven before pouring into the hopper. The optimum processing parameters for PA66 injection molding gears were set as 280 ℃, 80 ℃, 60 s, and 0.35 % for nozzle temperature, mold temperature, cooling time, and N_2 content, respectively. Other parameters for operating conditions were also listed in Table 1 for the following experiment.

Table 1. Operating conditions of the microcellular injection molding process.

Parameter	POM/PA66	Unit
Nozzle temperature	210/280	℃
Mold temperature	80/80	℃
Cooling time	50/60	s
N_2 content	0.50/0.35	%
Injection flow rate	8-12/12-15	mm/s
Injection pressure	220/250	MPa
Injection volume	85-95/70-90	mm

The actual product picture is illustrated in Figure 1. There were 6 gates on the gear shaft, which were inllustrated in the gating system, and the standard accuracy was 120.60 mm in the cross direction and 20.50 mm in the flow direction. After employing the microcellular injection molding process, the foamed POM and PA66 gear parts obtained 5% and 10% average weight reduction when compared with their solid counterparts, respectively.

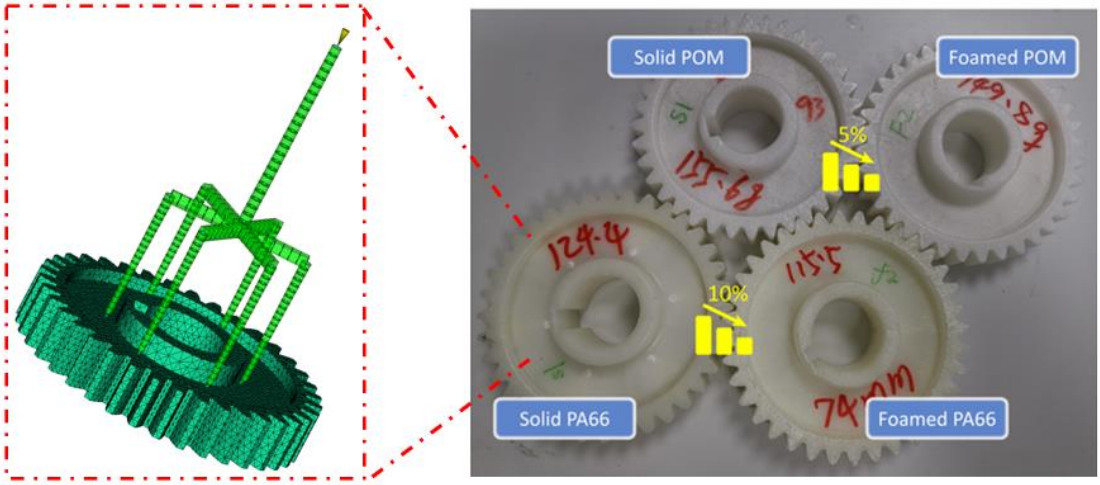

Figure 1. The actual product picture of the solid and foamed gears fabricated by POM and PA66.

2.3 Characterization

Differential scanning calorimeter (DSC) measurements were performed via a DSC 200F3 (NETZSCH) to quantitatively reveal the thermal behavior of the POM and PA66 raw materials. Approximately 7.5 mg POM samples were encapsulated in a standard aluminum pan and were heated to 230 ℃ at the heating rate of 10 ℃/min in a nitrogen atmosphere. After keeping the temperature at 230 ℃ for five minutes to remove the previous thermal history, the samples were cooled to ambient temperature and heated to 230 ℃ again at the same scanning rate of 10 ℃/min. The testing conditions of PA66 samples were the same as POM except for the heating temperature, which was heated to 300 ℃.

Thermogravimetric analysis (TGA) was adopted to reveal the decomposition behavior of the POM and PA66 raw materials on a TG 209 F3 (NETZSCH). After being dried in a vacuum oven for 2 hours at the temperature of 80 ℃, 3.7 mg POM samples and 3.8 mg PA66 samples were loaded followed by gradual heating from 30 ℃ to 410 ℃ and 550 ℃ respectively, with a heating rate of 10 ℃/min. The weight loss of the samples was recorded.

The microstructures of the prepared samples were imaged using a fully digital LEO GEMINI 1530 scanning electron microscopy (SEM) with an accelerating voltage of 15 kV. Prior to SEM imaging, the formed samples were cut into the cross-section and longitudinal sections using a band-sawing machine. The sawn-off pieces were subsequently fractured in liquid nitrogen to obtain the specimens. All specimens were sputtered with a thin film of gold for 120 s.

The 3-D profiles of the solid and foamed samples were both scanned through a white light interferometer (Atometrics), with a magnification of 20 times. Three different sampling locations were opted to calculate the average surface roughness, and the 3-D profiles of each gear sample were photographed.

The tensile and compression test experiments of both solid and foamed samples were carried out on a mechanical testing machine (Instron 5967). Tensile specimens were positioned between static and movable clamps and stretched at a crosshead speed of 50 mm/min till fracture, and compression specimens were compreesed at a crosshead speed of 1mm/min till the strain reached 20%. The average data and standard deviations were obtained from five repetitive experiments

3. Results and Discussion

3.1 Thermal Properties

The thermal properties of POM and PA66 raw materials would significantly affect the processing conditions and shrinkage behavior during the cooling period after the products were fabricated. It is essential to guarantee that both gears were prepared in the proper situation, and subsequently underwent the same shrinkage process[27]. The TGA measurement was used to investigate the decomposition behavior of the raw materials since POM and PA66 require harsh processing conditions in injection molding. The degradation temperature, degradation time, and char residual of raw materials are important for directing the processing conditions. Figure 2 shows the mass change of POM and PA66 raw materials by the TGA tests as the temperatures increase. As shown in Figure 2 (a), the POM started decomposition at 345.0 ℃, and the POM

weight residual decreased to 0 at 422.8 ℃. Regarding PA66, the raw material begins decomposing at 385.0 ℃. DTG curves are obtained based on the TG results of POM and PA66, the peak point of the DTG curve corresponds to the inflection point from the TG curve and the Δm value of the DTG peak indicates the maximum decomposition rate. It was found that the maximum Δm value of POM is higher than that of PA66, which means that the decomposition trend of PA66 is steeper than that of POM.

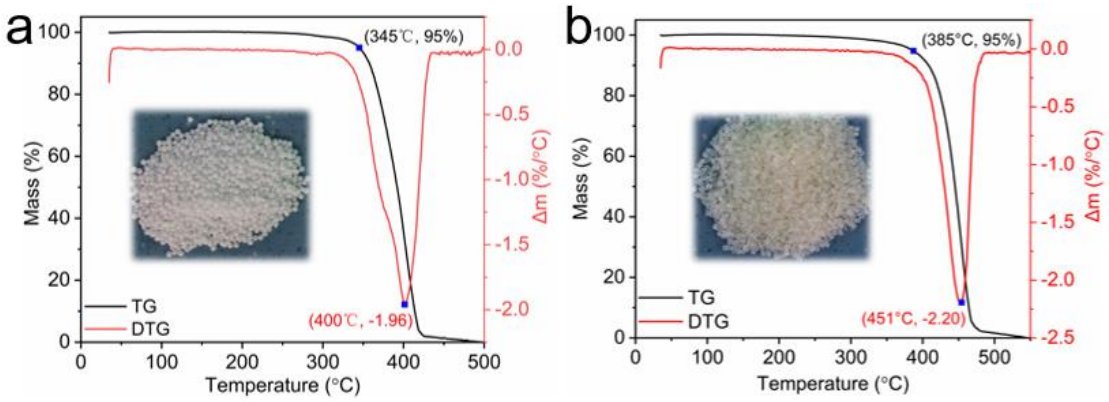

Figure 2. TGA weight percent curves of (a) raw POM and (b) raw PA66 material.

Figure 3 shows the first cooling and second heating cycles of POM and PA66, respectively, in the DSC measurement. The cooling traces with exothermic peaks revealed that the crystallization temperatures (T_c) of POM and PA66 were 146.3 ℃ and 136.8 ℃, respectively. In addition, the melting temperatures (T_m) of POM and PA66 were 165.9 ℃ and 197.8 ℃, respectively, obtained through the endothermic peak on heating traces. It was found that the PA66 has a much higher melting temperature and degradation temperature than the POM, which makes the processing temperature of PA66 material much higher than POM. Accordingly, the cooling time set in the preparation of PA66 gears should be longer than that for preparing POM gears, as noted in Table 1, which ensured that both gears were completely cooled in the mold cavity.

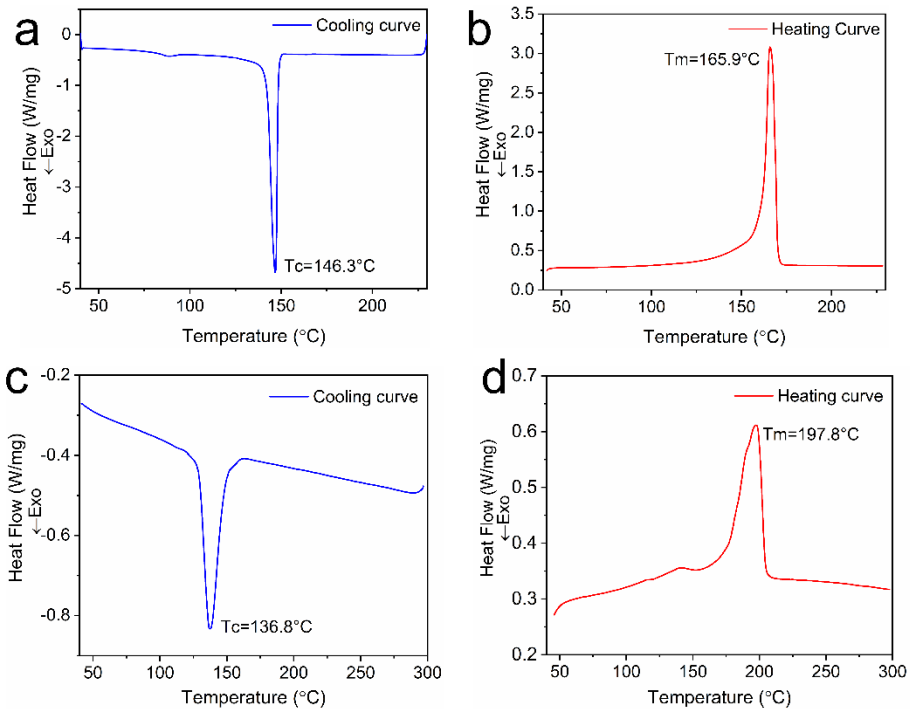

Figure 3. DSC results of pure POM and PA66 raw materials: (a) first cooling curve of POM (b) second heating curve of POM (c) first cooling curve of PA66 and (d) second heating curve of PA66.

In addition, the crystallinity of the raw materials was calculated based on the DSC curves by using:

$$X_c = \frac{\Delta H_f}{\Delta H_f^*} \times 100\% \quad (1)$$

Where ΔH_f represents the measured enthalpies of melting crystallization during the DSC heating scan, and ΔH_f^* is the melting enthalpy of 100% crystalline raw material. As for POM, the referred ΔH_f was 123.5 J/g, and the ΔH_f^* was 320 J/g, which led to the crystallinity (X_c) of 38.6 %. Moreover, the ΔH_f and ΔH_f^* of the related PA66 were 29.44 J/g and 195 J/g, calculating the crystallinity (X_c) to be 15.1%. The final physical performances of the molded parts are sensitive to the crystallinity degree[28], especially for the cell morphology and shrinkage ratio affected by the flow-induced crystallinity mechanism.

3.2 Cell Morphology of Microcellular Injection Molded Gears

The cell morphology of the microcellular injection molded POM and PA66 gears with six gates were observed using SEM at the location near the gate and far from the gate. As illustrated in Figure 4 (a), there was a distinct porous layer in the middle of the cross-section, with numerous bubbles formed in the layer. However, there was no clear boundary between the solid skin layers and porous core layer at the location far from the gate, as presented in Figure 4 (b), with fewer cells in the core layer. This was because the polymer near the gate was injected at the last where a higher temperature and lower pressure drop could be maintained. This is conducive to cell growth but has an adverse effect on cell nucleation. When the melt was first injected into the cold cavity, it would experience a long flow distance and rapid cooling which resulted in a thick skin layer[29]. Owing to the high crystallinity degree of POM material, the entanglements of the molecular chain ends enhanced the polymer stiffness[30], which inhibited the growth of internal bubbles in the core region of POM gears. Compared to POM gears, the micron-sized cells formed in the microcellular injection molded PA66 gears were more abundant, as shown in Figure 4 (c). There was more gas dissolved into the polymer[31], which accounted for the weight reduction difference between the foamed POM and foamed PA66. Moreover, most cells in PA66 gears had spherical shapes except for a proportion of ellipsoidal cells, which were deformed due to the flow of the melt during the filling process[26,32]. As the melting polymer traveled a long distance to the edge of the PA66 gear, the gas in the melt flow front was escaping

rapidly and there was a lack of gas barrier in the skin layer. Therefore, almost no bubbles were formed at the location far from the gate (Figure 4 (d)), which was consistent with the morphology results shown in Figure 4 (b).

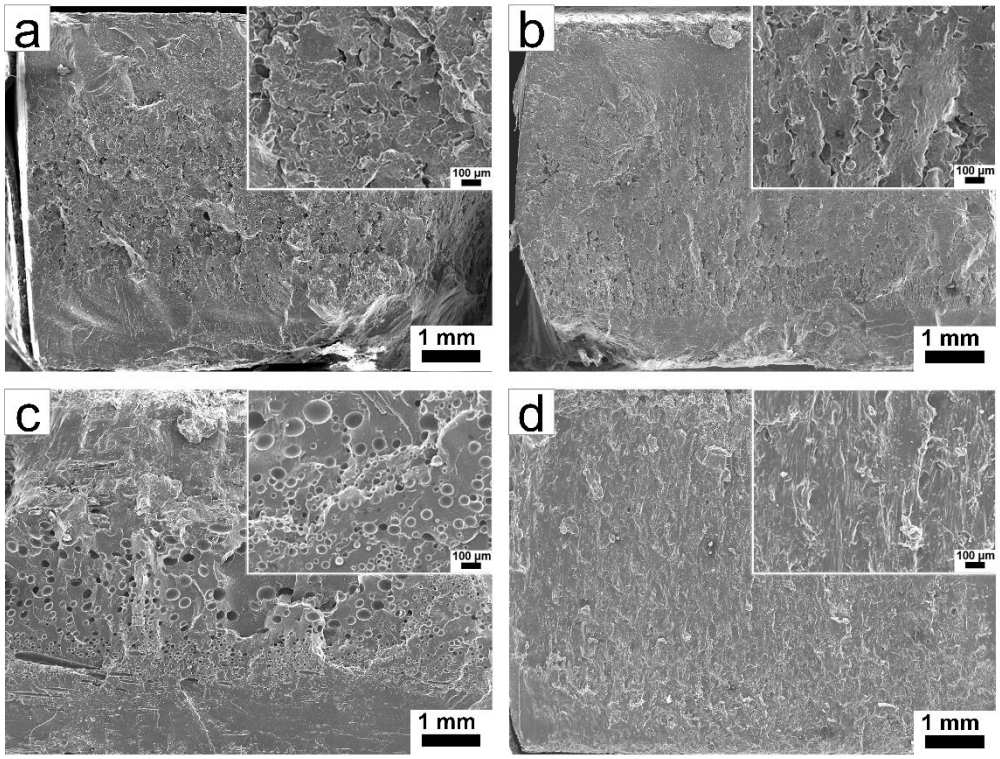

Figure 4. Cell morphology of the microcellular injection molded POM and PA66: (a) POM gear near the gate (b) POM gear far from the gate (c) PA66 gear near the gate (d) PA66 gear far from the gate.

For comparison, the cell size and cell density were measured from the SEM images of foamed POM and PA66 gear parts to quantitively evaluate the structural difference in different locations. As shown in Figure 5(a), the cell diameter in the location near the gate is greater than the location far from the gate. For instance, the average cell size of foamed POM gear part at the region near the gate was about 44 μm which is larger than the cells located far from the gate which was about 35 μm. This was because the

region near the gate was injected at the last and a higher temperature and lower pressure difference could be maintained, which is favorable for cell growth. On the other hand, since the melt mass-flow rates of PA66 and POM are 13 g/10min and 5.2 g/10min, the cell density of PA66 was greater than that of POM due to the higher melt strength as shown in Figure 5(b).

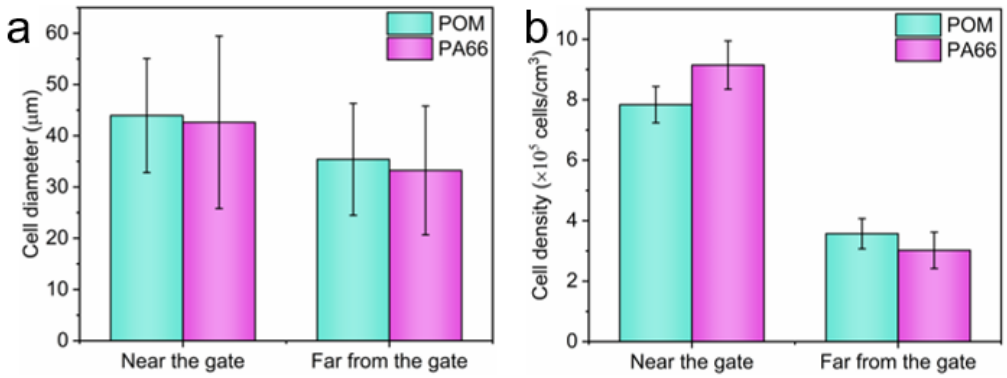

Figure 5. Statistical cell morphology data at the location near the gate and far from the gate of the foamed POM and PA66 gear parts: (a) cell diameter (b) cell density.

3.3 3D surface profiles

The 3D surface profiles of solid and foamed gear samples were characterized using a white-light interferometer and the results were illustrated in Figure 6. It was found that the solid injection molded samples exhibit smoother surface appearances than the foamed parts, with few appearance defects on the surface[33]. However, the surface appearance was still not flattened enough with many hollows distributed on the local surface, as illustrated in Figure 6(a) and Figure 6(c). Compared to the solid injection molded gears, 3D surface profiles of the foamed gears became more complicated[34]. Some tiny gas marks and scratches showed up like cloud clusters on the surface of microcellular POM and PA66 gear parts, and similar surface performances were shown

in Figure 6(b) and Figure 6(d). These results were attributed to the gas escaping from the ruptured micron-sized cells, the escaped nitrogen was trapped within the limited space at the gear-mold interface, leading to minor swirl marks and silver streaks on the surface of the microcellular injection molded gear samples. Meanwhile, the shear force between the melting polymer and the mold cavity was reduced with good melt fluidity, which significantly improves or even eliminates the appearance defects of the microcellular injection molded parts[26]. Since the crystallization temperature and crystallization rate of POM are higher than that of PA66, POM would crystallize and solidify faster than PA66 when the molten polymer is injected into the mold cavity, which leads to a slightly worse surface quality of solid POM than that of solid PA66 parts (Fig. 6 (c)).

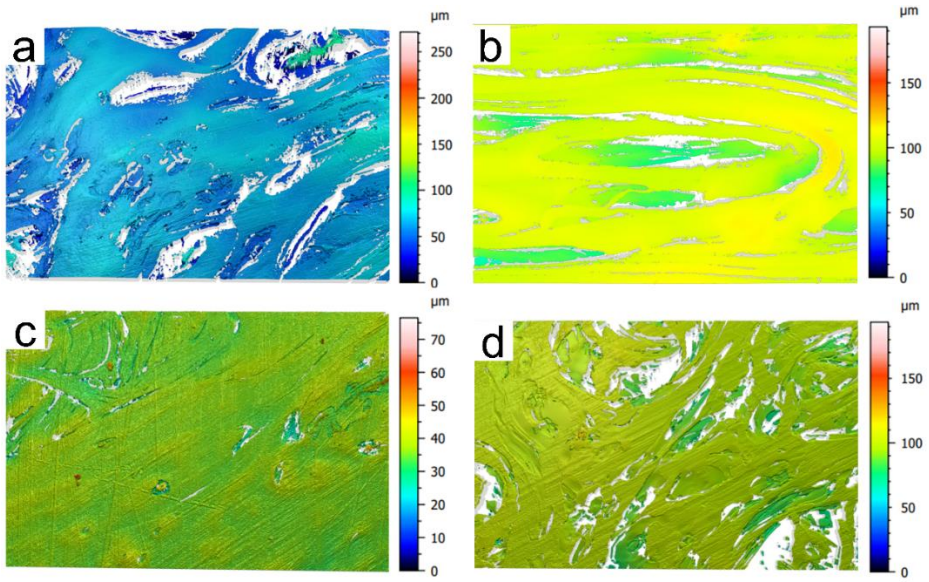

Figure 6. Comparison of 3-D profiles for (a) Solid POM (b) Foamed POM (c) Solid PA66 and (d) Foamed PA66.

To achieve a better comparison, five different locations on solid and foamed gear samples of POM and PA66 materials were selected to measure the average surface

roughness, and the results were presented in Figure 7. The surface roughness of the solid POM gear is 3.3 μm, although the foamed POM gear shows a 24% increase in surface roughness compared with the solid POM gear, which reached up to 4.1 μm, it still appears smooth and acceptable to the naked eye. When referring to the PA66 injection molded gears, the average surface roughness of the solid parts is 2.6 μm, while the foamed ones exhibit an average surface roughness of 3.2 μm, which is 23% rougher than the solid PA66 gear sample. Although the roughness of foamed gears was slightly increased, the overall flatness was remarkably improved compared with that of solid samples, which is beneficial to improve the application of foamed gears.

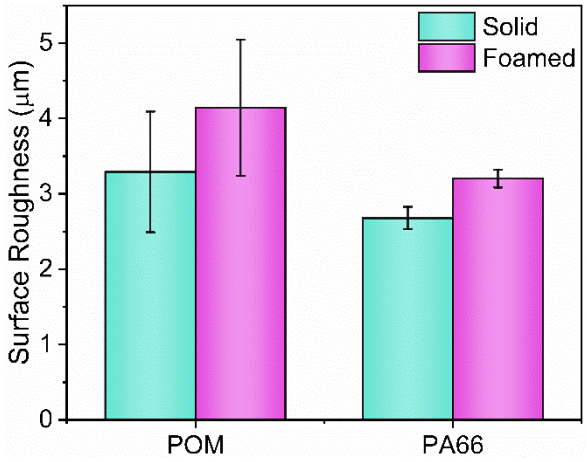

Figure 7. Surface roughness of the POM and PA66 samples.

3.4 Mechanical property

To compare the mechanical properties of solid/foamed POM and PA66 gear plastic parts, the Instron 5967 mechanical testing machine was used to test the tensile and compression properties of the gear parts. As shown in Figure 8, when the tensile force acts on the gear plastic, the stress and strain initially show a proportional relationship. With the further increase of the strain, the growth of the curve slows down.

The tensile strength of solid POM gear was 62 MPa, while it decreased to 50 MPa for foamed POM. The corresponding tensile modulus also has a small decrease. On the other hand, the PA66 gear parts showed good toughness and greater elongation at break than POM gear parts. The tensile modulus of solid and foamed PA66 gear plastic parts were 2.68 GPa and 1.65 GPa, respectively. When subjected to compression, the trends of compressive properties of solid and foamed POM and PA66 gear parts are consistent with the tensile properties as shown in Figures 8 (c) and 8 (d).

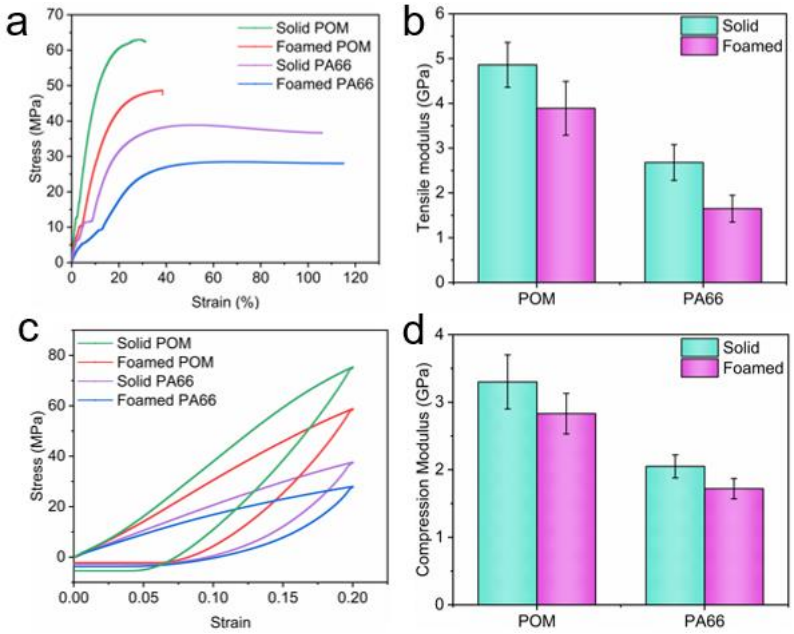

Figure. 8 Comparison of mechanical properties of POM and PA66 gears under different process conditions: (a) tensile stress-strain curves (b) tensile modulus (c) compressive stress-strain curves (d) compressive modulus.

3.5 Shrinkage ratio

Shrinkage is a common phenomenon in injection molded products as the temperature drops, usually, the injection product would shrink to its final state after placing in the ambient temperature for 48 hours since the product was taken out from

the mold cavity. The shrinkage ratios of solid and foamed gear samples were calculated with the following formula:

$$S(\%) = \frac{M - P}{M} \times 100\% \quad (2)$$

Where S represents the calculated shrinkage ratio of the injection gear samples, M is the mold dimension, and P indicates the dimension of the injection products after cooling for 48 hours.

The thickness and diameter of the injection molded gears with six gates were measured in both flow direction and cross-section perpendicular to the flow direction, and five different locations on a gear sample were selected to calculate the average shrinkage ratio. As illustrated in Figure 9 (a), the solid POM gear shows 0.31 ‰ shrinkage in the flow direction and 0.23 ‰ shrinkage in the cross direction. These results indicate that the temperature of the polymer in the melt flow front is much higher than the polymer at the edge of the gear after traveling a long distance. As such, the shrinkage ratio in the flow direction is larger than that in the cross direction. When compared to the foamed POM gear, there is a noticeable decline in the shrinkage ratio both in the flow direction and the cross direction. It is worth mentioning that the shrinkage ratio in the cross direction decreased from 0.23 ‰ to 0.17 ‰ when they were molded using microcellular injection molding. For crystalline polymers, the crystallization process would trigger the polymer molecular chains to arrange orderly and densely[35,36], which led to the increase of polymer density in the macroscopic view[37]. Therefore, the higher the crystallinity degree of the polymer, the greater the

density of the polymer itself. Notably, the crystallinity of the polymer is closely related to its density[30,38].

The higher crystallinity of POM caused the tighter molecular chain arrangement than PA66. As the density increase due to the arrangement of polymer molecular chains, the overall volume of the polymer will inevitably shrink after injecting specific volume of melting polymer. Accordingly, the solid PA66 gear presents 0.18 ‰ shrinkage ratio in the flow direction and 0.12 ‰ in the cross direction, which demonstrates that the PA66 raw materials possess a lower shrinkage rate than the POM raw materials. Meanwhile, the foamed PA66 gear shows a more significant dimensional accuracy improvement, with 0.13 ‰ shrinkage ratio in the flow direction and 0.07 ‰ in the cross direction, making its accuracy close to the mold cavity dimension.

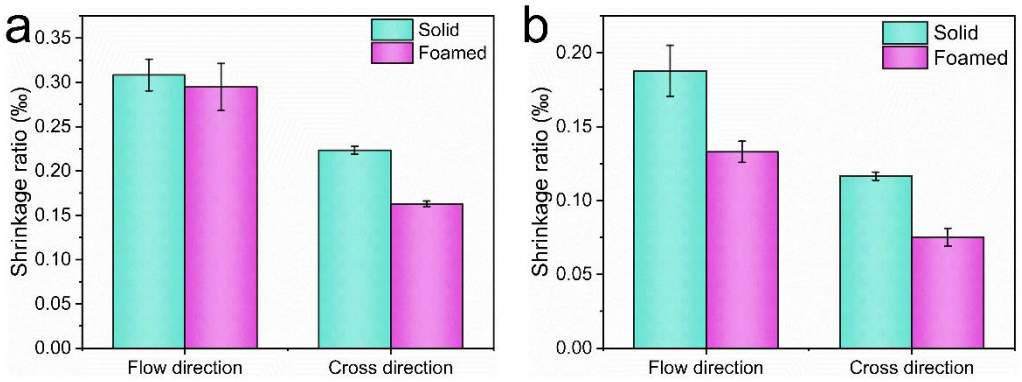

Figure 9. Shrinkage ratios in the flow direction and the cross direction for (a) POM samples and (b) PA66 samples.

The improvement in dimensional accuracy of the microcellular injection molded gears was mainly attributed to the special sandwich structure comprised of numerous micron-sized cells in the core region. As depicted in Figure 10, there was a clear

contraction in the flow direction of the solid gear due to the higher temperature of the latest injected melting polymer. The entire gear sample would undergo a contraction process as the temperature drops from the cavity temperature to the ambient temperature, the long polymer chains tended to rearrange themselves into crystalline structures when the solidification began[36], and the slight shrinkage would persist up to 48 hours after the gears taking out from the mold cavity. During the cooling process, the shrinkage stress forced the polymer at the part edge to contract inward. The existence of micron-sized cells in the microcellular injection molded foamed parts would offset part of the inward shrinkage stress, and restrict the chain movements, which provided a barrier against the recrystallization activity during the re-solidification process[20], thus, reducing the shrinkage degree of the foamed gear parts. Therefore, the shrinkage ratios of microcellular injection molded foamed parts should be smaller in both flow direction and cross direction. However, the micro-cells presented in the foamed parts may also shrink due to the gradual diffusion of gas at a critical point. Hence, there might be an optimum void-to-solid ratio that reaches a desirable balance between polymer shrinkage and cell expansion.

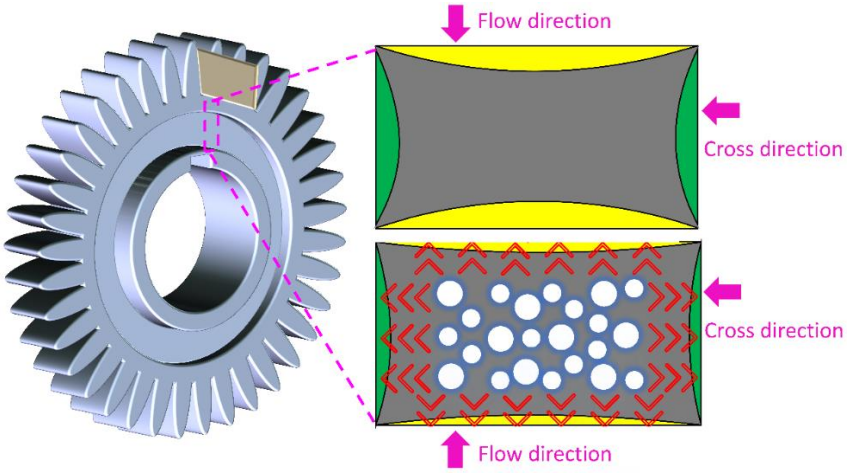

Figure 10. Schematic of the shrinkage ratio decreasing mechanism by a microcellular structure with foam bubbles.

According to the above results, PA66 foamed gear parts presented better dimensional accuracy compared to POM counterparts due to its lower polymer arrangement during cooling. Taking PA66 as an example, the effect of injection volume (reflecting the void-to-solid ratio of foamed parts) on the shrinkage ratio was investigated. The contractions of the foamed parts in both flow direction and cross direction were measured as the injection volume varied in the range of 65 to 85 millimeters. As illustrated in Figure 11, the shrinkage ratio in the flow direction was higher than in the cross direction under all injection volume conditions, and the shrinkage ratio in the two directions kept the same tendency. When the injection volume was between 74 mm and 85 mm, increasing bubbles substituted for the solid polymer as the injection volume decreased, but the quantity of micron-sized cells was limited at the very beginning, so the shrinkage ratio showed a slight increase in both directions. As the injection volume was reduced to 74 mm, increasing N_2 volume provides more cell nucleation points, and high-density cells with fine cell structure were formed to raise the specific volume of the homogeneous system when compared to the solid counterpart. The shrinkage ratio exhibited a marked downward trend due to the rising expansion force, which offset the inward shrinkage stress to the greatest extent[20]. It is demonstrated that the lowest shrinkage ratio was obtained at the injection volume of 74 mm, with a shrinkage ratio of 0.043‰ in the flow direction and 0.037‰ in the cross

direction. However, the shrinkage ratio changed to an increasing trend when the injection volume was lower than 74 mm. Further increase in void-to-solid ratio caused the over-expansion of internal bubbles in the plastic part[39,40], which resulted in the coalescence and collapse of bubbles due to the diffusion and escaping of gas from the cells. When the injection volume was further declined to 65 mm, a short-shot phenomenon occurred which resulted in severe gas escaping during the cooling period [41,42], thus, significantly affecting the dimension accuracy of the foamed PA66 gears. These results proved that there was an optimum point for the foamed PA66 gear parts to obtain the lowest shrinkage ratio when the maximum foaming ratio was realized by controlling the injection volume.

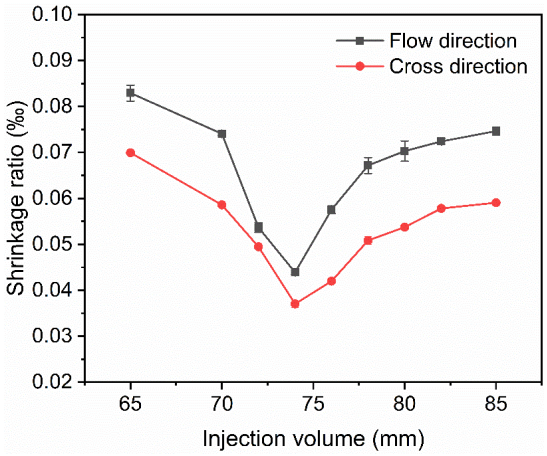

Figure 11. The shrinkage ratio of foamed PA66 gears in flow direction and cross direction under different injection volumes.

Figure 12 shows the cell morphology of the foamed PA66 gear parts when the injection volume was set at 85 mm, 80 mm, 74 mm, 70 mm, and 65 mm. It was found that the part has a small cell size at a high injection volume. With the decrease in injection volume, the number of cells increased, and the diameter of bubble holes

increased. When the injection volume was 74 mm, dense cells were formed in the core layer of foamed PA66 gear parts, with a diameter of 48 μm, as shown in Figure 12(c). At this time, the cells could provide the maximum expansion effect, and the foamed parts also obtained the highest dimensional accuracy. When the injection volume was further reduced, excess gas caused cell merge and rupture, leading to a great increase of cell diameter. When the injection volume was 65 mm, the cell diameter reached 550 μm, as illustrated in Figure 12(e). At this time, the gear parts had a short-shot phenomenon, resulting in the rise of shrinkage rate.

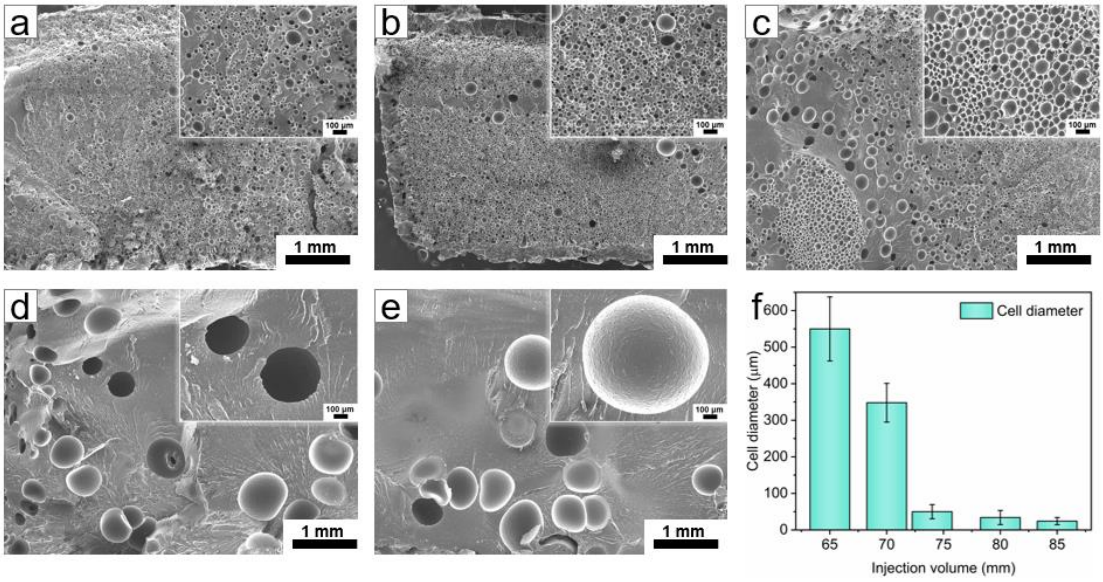

Fig. 12 Cell morphology of foamed PA66 gear parts under different injection volumes: (a) 85 mm (b) 80 mm (c) 74 mm (d) 70 mm (e) 65 mm (f) cell diameter.

4. Conclusion

Microcellular injection molding of POM and PA66 gear parts with nitrogen as the blowing agent was studied to seek high dimensional accuracy. The number of cells in foamed POM gear was smaller and the morphology was more irregular than the cells

in foamed PA66 gear, which achieved an average weight reduction of 5%, compared with a 10% weight reduction of PA66 foamed gear parts. In addition, the solid skin layer was much thicker in the region far from the gate than the one near the gate due to the high-temperature variation and pressure drop. Although the foamed gear parts exhibited a minor rougher surface appearance than the solid counterparts, the overall flatness of foamed ones was remarkably improved. In comparison with the solid gear parts, the foamed counterparts showed a lower shrinkage ratio in both flow direction and cross direction due to the cell expansion, which offset part of the inward shrinkage stress, especially in the cross direction. The shrinkage ratio of injection gear parts was notably determined by the differences in crystallinity degree of materials, PA66 gear parts, indicating a lower shrinkage ratio than the POM counterparts. In addition, the lowest shrinkage ratio was obtained at the injection volume of 74 mm, when the polymer approached the maximum foaming ratio, with a shrinkage ratio of 0.043‰ in the flow direction and 0.037‰ in the cross direction. This study offers essential data and contributes to directing microcellular injection molding thick-wall products, and gives a further exploration into the effect of the foaming process on improving dimensional accuracy.

Acknowledgments

The authors would like to acknowledge the financial support of the National Natural Science Foundation of China (52173049), the China 111 project (D18023), and the China Postdoctoral Science Foundation (2021M101797).

References

[1] Volpe, V., Lanzillo, S., Affinita, G., Villacci, B., Macchiarolo, I. & Pantani, R., *Polymers* **2019**, 11, 2, 326.

[2] Trobentar, B., Kulovec, S., Hlebanja, G. & Glodež, S. J. E. F. A., *Journal Pre-proofs* **2020**, 111, 104496.

[3] Raghuraman, N., Houser, D. & Wright, Z. H., *Gear Solutions* **2017**.

[4] Singh, P. K. & Singh, A. K., *Tribology International* **2018**, 118, 264.

[5] Pogačnik, A. & Kalin, M., *Wear* **2012**, 290, 140.

[6] Li, W., Wood, A., Weidig, R. & Mao, K., *Wear* **2011**, 271, 9-10, 2176.

[7] Mi, H. Y., Jing, X., Salick, M. R., Peng, X. F. & Turng, L. S., *Polymer Engineering Science* **2014**, 54, 12, 2947.

[8] Ni, G.-L., Zhu, X., Mi, H.-Y., Feng, P.-Y., Li, J., Jing, X., Dong, B., Liu, C. & Shen, C., *Nano Energy* **2021**, 87, 106148.

[9] Sun, X. & Turng, L. S., *Polymer Engineering Science* **2014**, 54, 4, 899.

[10] Suh, N. Gardmer Publications, Inc, **1996**.

[11] Evans, N. T., Torstrick, F. B., Lee, C. S., Dupont, K. M., Safranski, D. L., Chang, W. A., Macedo, A. E., Lin, A. S., Boothby, J. M. & Whittingslow, D. C., *Acta biomaterialia* **2015**, 13, 159.

[12] Yang, Q., Zhang, G., Ma, Z., Li, J. & Fan, X., *Journal of Applied Polymer Science* **2015**, 132, 39, 42576.

[13] Xie, P., Wu, G., Cao, Z., Han, Z., Zhang, Y., An, Y. & Yang, W., *Polymers* **2018**, 10, 5, 554.

[14] Zhiguo, M., Xianzhang, S., Yulong, H., Jun, Z., Ming, H., Yongzhi, L., Chuntai, L. J. A. C. & Materials, H., *Adv Compos Hybrid Mater.* **2022,** 7, 1.

[15] Zhao, J., Guo, C., Zuo, X., Román, A. J., Nie, Y., Su, D.-X., Turng, L.-S., Osswald, T. A., Cheng, G., Chen, W. J. A. C. & Materials, H., *Adv Compos Hybrid Mater.* **2022**, 5, 4, 2964.

[16] Guo, W., Yang, Q., Mao, H., Meng, Z., Hua, L. & He, B., *Polymers* **2019**, 11, 5, 778.

[17] Chen, J., Chi, W., Dang, K., Xie, P. & Yang, W., *Journal of Applied Polymer Science* **2021**, 138, 33, 50828.

[18] Hwang, S.-S. & Ke, Z.-S., *International Communications in Heat and Mass Transfer* **2008**, 35, 3, 263.

[19] Kim, H. K., Sohn, J. S., Ryu, Y., Kim, S. W. & Cha, S. W., *Polymers* **2019**, 11, 2, 360.

[20] Zafar, R., Lee, K. S., Kim, H. B., Jeon, B. J. & Cha, S. W., *Polymer-Plastics Technology Engineering* **2008**, 47, 11, 1187.

[21] Clausi, M., Zahid, M., Shayganpour, A. & Bayer, I. S., *Advanced Composites Hybrid Materials* **2022,** 5, 2, 798.

[22] Cui, Z., Zhao, M., Wu, J., Liu, X., Si, J. & Wang, Q., *Advanced Composites Hybrid Materials* **2022**, 1.

[23] He, B., Xu, Y., Zhu, J., Zhang, X. J. A. C. & Materials, H., *Advanced Composites and Hybrid Materials* **2021**, 4, 4, 1146.

[24] Kramschuster, A., Cavitt, R., Ermer, D., Chen, Z. & Turng, L. S., *Polymer Engineering Science* **2005**, 45, 10, 1408.
[25] Lotti, C., Ueki, M. & Bretas, R., *Journal of Injection Molding Technology* **2002**, 6, 3, 157.
[26] Guo, W., Mao, H., Li, B. & Guo, X., *Procedia Engineering* **2014**, 81.
[27] Sykutera, D., Czyżewski, P. & Szewczykowski, P., *Materials* **2021**, 14, 15, 4199.
[28] Santis, F. D., Pantani, R., Speranza, V. & Titomanlio, G., *Industrial engineering chemistry research* **2010**, 49, 5, 2469.
[29] Ma, Z., Zhang, G., Yang, Q., Shi, X., Li, J., Zhang, H. & Qin, J., *The Journal of Supercritical Fluids* **2018**, 140, 116.
[30] Kościuszko, A., Marciniak, D. & Sykutera, D., *Materials* **2020**, 14, 1, 22.
[31] Ding, Y., Vyas, C., Bakker, O., Hinduja, S. & Bartolo, P., Polymers **2022**, 14, 19, 4215.
[32] Meister, S. & Drummer, D. J. P. T., *Polymer Testing* **2013**, 32, 2, 432.
[33] Yang, J., Xie, J., Ji, K., Wang, X., Jiao, X., Xu, Z., Zhao, P. J. J. o. M. R. & Technology, *Journal of materials research and technology* **2022**, 19, 1678.
[34] Peng, J., Srithep, Y., Wang, J., Yu, E., Turng, L.-S. & Peng, X.-F. J. J. o. c. p., *Journal of Cellular Plastics* **2013**, 49, 1, 33.
[35] Di, Y., Iannace, S., Di Maio, E. & Nicolais, L., *Macromolecular materials engineering* **2005**, 290, 11, 1083.
[36] Gan, H., Kabe, T., Kimura, S., Hikima, T., Takata, M. & Iwata, T., *Polymer* **2019**, 172, 7.
[37] Nofar, M., Batı, B., Küçük, E. B. & Jalali, A., *The Journal of Supercritical Fluids* **2020**, 160, 104816.
[38] Menyhárd, A., Faludi, G. & Varga, J., *Journal of thermal analysis calorimetry* **2008**, 93, 3, 937.
[39] Xu, Z., Wang, G., Zhao, J., Zhang, A., Dong, G. & Zhao, G., *Journal of CO2 Utilization* **2022**, 62, 102076.
[40] Chen, P., Gao, X., Zhao, L., Xu, Z., Li, N., Pan, X., Dai, J. & Hu, D., *Polymer Degradation Stability* **2022**, 197, 109844.
[41] Hou, J., Zhao, G., Wang, G., Dong, G. & Xu, J., *Materials Design* **2017**, 127, 115.
[42] Feng, Y.-T., Wang, L., Mi, H.-Y., Gu, L., Dong, B., Liu, C. & Shen, C., *Advanced Engineering Materials* **2021**, 24, 3.